Physics and Imaging in Radiation Oncology 26 (2023) 100434

Contents lists available at ScienceDirect

Physics and Imaging in Radiation Oncology

journal homepage: www.sciencedirect.com/journal/physics-and-imaging-in-radiation-oncology

Original Research Article

Feasibility of online radial magnetic resonance imaging for adaptive radiotherapy of pancreatic tumors

Guus Grimbergen *, Hidde Eijkelenkamp, Jonna K. van Vulpen, Saskia van de Ven, Bas W. Raaymakers, Martijn P.W. Intven, Gert J. Meijer

Department of Radiation Oncology, University Medical Center Utrecht, the Netherlands

ARTICLE INFO

Keywords:
Pancreatic cancer
MR-guided SBRT
online adaptive RT
radial MRI

ABSTRACT

Background and purpose: Online adaptive magnetic resonance (MR)-guided treatment planning for pancreatic tumors on 1.5T systems typically employs Cartesian 3D T_2w magnetic resonance imaging (MRI). The main disadvantage of this sequence is that respiratory motion results in substantial blurring in the abdomen, which can hamper delineation accuracy. This study investigated the use of two motion-robust radial MRI sequences as main delineation scan for pancreatic MR-guided radiotherapy.

Materials and methods: Twelve patients with pancreatic tumors were imaged with a 3D T_2w scan, a Periodically Rotated Overlapping ParallEL Lines with Enhanced Reconstruction (PROPELLER) scan (partially overlapping strips), and a 3D Vane scan (stack-of-stars), on a 1.5T MR-Linac under abdominal compression. The scans were assessed by three radiation oncologists for their suitability for online adaptive delineation. A quantitative comparison was made for gradient entropy and the effect of motion on apparent target position.

Results: The PROPELLER scans were selected as first preference in 56% of the cases, the 3D T_2w in 42% and the 3D Vane in 3%. PROPELLER scans sometimes contained a large interslice variation which would have compromised delineation. Gradient entropy was significantly higher in 3D T_2w patient scans. The apparent target position was more sensitive to motion amplitude in the PROPELLER scans, but substantial offsets did not occur under 10 mm peak-to-peak.

Conclusion: PROPELLER MRI may be a superior imaging sequence for pancreatic MRgRT compared to standard Cartesian sequences. The large interslice variation should be mitigated through further sequence optimization before PROPELLER can be adopted for online treatment adaptation.

1. Introduction

With the introduction of magnetic resonance linear accelerator (MR-Linac) systems, radiotherapy for upper abdominal tumors can be conducted using an MR-guided online adaptive procedure [1,2]. During this procedure, treatment plans can be re-adapted to the anatomy at every fraction based on MR imaging, a modality with a vastly superior soft tissue contrast and flexibility compared to computed tomography (CT) imaging of conventional radiotherapy. This introduction of MR-guided radiotherapy (MRgRT) has made high dose, hypofractionated stereotactic body radiotherapy (SBRT) feasible for pancreatic tumors [3–8], which can potentially lead to improved survival [9].

In MRgRT on a 1.5T MR-Linac, the imaging sequences typically used for online plan adaptation are based on 3D, turbo spin echo (TSE), Cartesian *k*-space sampling patterns. These sequences have long been the standard in many routine radiological and radiotherapeutic applications, and therefore trained clinicians are used to the imaging contrast of these scans. Moreover, 3D imaging can be acquired with a high through-plane resolution, which facilitates structure contouring in radiotherapy as there is less structural variation from slice to slice. A substantial downside however, especially in abdominal imaging, is sensitivity to motion, which causes blurring and ghosting artifacts [10]. This can be a significant concern for MRgRT, as blurred structures may hamper accurate delineation of the tumor and organs at risk (OAR).

In contrast to Cartesian MRI, radial sampling schemes are much less sensitive to motion and might therefore reduce delineation uncertainty in the upper abdomen. Two examples of motion-robust radial MRI sequences are PROPELLER (Periodically Rotated Overlapping ParallEL Lines with Enhanced Reconstruction) [11] and 3D Vane. PROPELLER, also known as MultiVane or BLADE, acquires multiple partially

* Corresponding author at: Department of Radiation Oncology, University Medical Center Utrecht, Heidelberglaan 100, 3584CX Utrecht, the Netherlands.
E-mail address: g.grimbergen@umcutrecht.nl (G. Grimbergen).

https://doi.org/10.1016/j.phro.2023.100434
Received 16 March 2023; Received in revised form 22 March 2023; Accepted 22 March 2023
Available online 25 March 2023

overlapping strips of phase encoding lines (so-called blades), each rotated around the center of *k*-space. In diagnostic radiology, PROPELLER MRI is a popular sequence for motion-robust T_2-weighted imaging of the abdomen [12–15], but also when there is risk of bulk motion, like in the brain [16–19] and pediatric imaging [20,21].However, the application of PROPELLER in the radiotherapeutic setting has as of yet not been investigated. In 3D Vane, *k*-space is sampled in a radial stack-of-stars pattern. While this sequence cannot provide T_2w contrast, it can acquire images in 3D fashion, rather than as multiple 2D slices such as PROPELLER. This results in the same high through-plane resolution as in conventional 3D Cartesian sequences.

This study qualitatively and quantitatively investigated the feasibility of employing radial MRI sequences, specifically PROPELLER and 3D Vane, for online contour adaptation during MR-guided radiotherapy of pancreatic tumors.

2. Materials & methods

2.1. Patients material

Twelve consecutive patients that underwent MRgRT for pancreatic tumors between January and June 2022 were included. Patients provided informed consent through the prospective Multi-OutcoMe EvaluatioN of radiation Therapy Using the MR-Linac (MOMENTUM) study (NCT04075305). A summary of the patient characteristics is shown in Supplementary Table S1.

All patients were treated with a hypofractionated stereotactic body radiotherapy (SBRT) regimen (five fractions of 8 Gy) on an Elekta Unity (Elekta AB, Stockholm, Sweden) MR-Linac, a 7 MV linear accelerator combined with a 1.5T wide bore MRI scanner. During treatment, abdominal compression was applied with a custom fitted Neofrakt abdominal corset (Spronken Orthopedie NV, Genk, Belgium) to mitigate intrafraction motion [22].

2.2. Imaging

For each patient, three imaging sequences were acquired during a MRgRT treatment fraction: a multi-slice 2D (M2D), T_2w PROPELLER scan, a 3D Vane scan and a Cartesian 3D T_2w scan. Imaging was performed using the standard clinical 8-channel receive coil array of the Elekta Unity system. The PROPELLER scan was acquired with a *k*-space coverage of 318%, as set by the Multivane percentage parameter (500%) in the 1.5T Philips MR system of the MR-Linac used in this study. Echo time (TE) and repetition time (TR) were 130 and 3000 ms. SENSE undersampling with factor 4 was employed to result in a total scan time of three minutes and 30 s.

The 3D Vane scan was acquired as a balanced gradient echo stack-of-stars sequence, with Cartesian ordering in the k_z direction. Here, TE and TR were 2.4 and 4.9 ms, and total imaging time was four minutes and 45 s. The 3D T_2w scan was a turbo spin echo (TSE) sequence with TE/TR of 124/1300 ms, and total imaging time of four minutes and four seconds. More details on the imaging sequence parameters are given in Table 1.

Table 1
Sequence parameters. TSE, turbo spin echo; bTFE, balanced turbo field echo; FOV, field of view; TE, echo time; TR, repetition time; FA, flip angle.

	3D T_2w	M2D PROPELLER	3D Vane
Scanning technique	TSE	TSE	bTFE
FOV (mm^3)	451 × 451 × 220	420 × 420 × 210	450 × 450 × 150
Voxel size (mm^2)	0.64 × 0.64	0.58 × 0.58	0.62 × 0.62
Slice thickness (mm)	2.0	3.6	3.0
TE/TR (ms)	124/1300	130/3000	2.4/4.9
FA (°)	90	90	50
Echo train length	100	45	n/a
Readout bandwidth (Hz/pixel)	820	352	718
Total scan time (min:sec)	4:04	3:30	4:45

2.3. Qualitative analysis

All scans were analyzed by three experts specialized in upper abdominal (MR-guided) radiotherapy: two radiation oncologists (SvdV, 9 years of experience and MPWI, 14 years of experience) and one radiation oncology resident (JKvV, 4 years of experience). Per patient, the observers were asked to independently rank the three scans in order of preference for use as main delineation scan in an online adaptive setting. Moreover, each scan was scored on three aspects: 1) in-plane tumor delimitability, i.e. the ability to differentiate and delineate the tumor border; 2) in-plane OAR delimitability, i.e. the ability to differentiate and delineate the borders of the critical OAR (e.g. duodenum, small bowel, stomach); 3) the level of image artifacts in the area in and around the tumor. These aspects were scored on a five-point scale, from 1 (worst) to 5 (best). Concrete examples of criteria for the different scores are in Supplementary Table S2.

2.4. Quantitative analysis

Gradient entropy is a quasi-objective image quality metric specifically related to motion artifacts [23]. Entropy is used here in the context of information theory. Gradient entropy postulates that an ideal image consists of areas of uniform gray values, separated by sharp edges. For such an image, the entropy of its gradient image is lower than for an image with blurry edges. Out of 24 metrics, gradient entropy was found to have the highest correlation with expert-based image quality scores [23]. The gradient entropy H of a 3D image is defined as:

$$H = -\sum_{i,j,k} g_{i,j,k} \log_2(g_{i,j,k}) \tag{1}$$

With $g_{i,j,k}$ the voxel values of the normalized gradient magnitude image:

$$g_{i,j,k} = \frac{|m_{i,j,k} * k|}{\sum_{i,j,k} |m_{i,j,k} * k|} + \varepsilon \tag{2}$$

With $m_{i,j,k}$ the gray values of the 3D image, k a 3-by-3-by-3 gradient kernel, and * the convolution operator. ε is a small constant to avoid taking the logarithm of 0. Formally, H is expressed in the unit bits. The gradient entropy was calculated for all patient scans.

Aside from delineation uncertainty due to blurring, the asymmetry of a patient's breathing pattern might lead to a change in the tumor's apparent position in the image. For ungated radiotherapy in free breathing, the delineated position of a moving tumor should correspond to the time-weighted average position during the respiratory cycle, also known as the midposition strategy [24]. Recently, Bertelsen et al. investigated the apparent position of a mobile target for 3D T_2w sequences in a phantom study, under different breathing conditions [25]. Based on their analysis, we extended this investigation to the PROPELLER and 3D Vane sequences.

Motion was simulated using the Quasar MRI 4D motion phantom (Modus Medical Devices, Ontario, Canada), an MRI-compatible phantom containing a mobile cylinder with a 30 mm sphere at the center. Both the sphere and the cylinder were filled with water, and the sphere was doped with $MnCl_2$ for a hypointense contrast with its surroundings. The cylinder was programmed to move with a $\cos^6$ function, with a period of 5 s, and an amplitude of 5 mm, 10 mm or 15 mm. For each amplitude, the function was offset with its average value to ensure the midposition of the target corresponds to its static position. The phantom was placed in the MR-Linac with the direction of motion parallel with the z-axis, i.e. the slice direction of the imaging sequences. As with the other experiments, the sequence parameters were kept identical to the patient acquisitions. For each sequence, the phantom was scanned in

static position, and with the phantom in motion with the three different amplitudes.

The target was automatically segmented in a single coronal slice of each image by k-means clustering with three clusters. As the target was always roughly in the center of the image, the cluster of the central voxel was assigned as the target segmentation, resulting in a binary mask of the target. To obtain a mask shape more reminiscent of human contouring, rough edges of the mask were smoothed by means of Gaussian filtering ($\sigma = 2$) and rebinarizing. The z-component of the mask's center of mass (COM) was extracted and compared to the static configuration, to quantify the offset of the target position as a result of motion.

2.5. Statistical analysis

Descriptive statistics were performed for the results of COM offset and observer preference. Differences between the gradient entropy and observer scores for tumor delimitability, OAR delimitability and artifacts were determined using the one-way analysis of variance (ANOVA) test and Tukey post hoc test ($p < 0.05$) in Statistical Package for Social Sciences (SPSS) version 25 (IBM, Armonk, NY).

3. Results

3.1. Qualitative analysis

Over the three observers, the 3D T_2w was in (rounded to the nearest percentage) 42% of the cases selected as the first preference, PROPELLER in 56%, and 3D Vane in 3% (Fig. 1a). In general, the PROPELLER images had sharper edges and improved visual definition of OARs (Fig. 2).

It was noted that in some PROPELLER scans, there was a large interslice variability in respiratory phase, causing structures to vary in position between slices. In two patients, the observers noted that this variability was so severe that it would have critically impeded the delineation process. This was the most commonly cited reason why the 3D T_2w scan was preferred above the PROPELLER scan, even if the PROPELLER scan was still of superior in-plane quality. Remarkable was that this interslice variability effect seemed very pronounced in some patients, but barely present in others (Fig. 3). The 3D Vane was indicated to be least preferred in 92% of the cases, with the most commonly cited reasons being the unconventional contrast of this sequence, and no contrast between tumor and healthy tissue.

The mean (SD) scores (higher is better) for tumor delimitability, OAR delimitability, and artifacts were: 3D T_2w: 3.0 (0.8), 3.0 (0.8), 3.3 (1.0); PROPELLER: 3.4 (0.9), 3.5 (0.8), 3.4 (0.8); 3D Vane: 2.1 (1.0), 2.6 (1.2), 3.8 (0.8) (Fig. 1b). Tumor delimitability scores were significantly higher in both the 3D T_2w scans and the PROPELLER scans compared to the 3D Vane scans (both $p < 0.001$), but PROPELLER was not scored significantly higher than 3D T_2w ($p = 0.122$). OAR delimitability was scored significantly higher in the PROPELLER scans than in the 3D T_2w scans ($p = 0.050$) and in the 3D Vane scans ($p < 0.001$). The observers noted that the scoring for tumor and OAR delimitability was often highly correlated, as both scores reflect the ability to distinct tumor from OARs.

3.2. Quantitative analysis

The mean (SD) gradient entropy in bits for each sequence was: 3D T_2w: 23.7 (0.3); PROPELLER: 22.9 (0.3); 3D Vane: 22.6 (0.3). Again, a lower gradient entropy signifies an image with sharper boundaries between structures. The gradient entropy in the 3D T_2w scans was significantly higher than in the other two sequences (both $p < 0.001$).

The center of mass offsets, relative to the midposition, are given in Fig. 4 as a function of motion amplitude. The acquired images, target segmentations and COM positions are given in Supplementary Figure S1. In all sequences, the center of mass of the segmented target showed a trend towards the exhale position as the motion amplitude increased past 10 mm. At 5 mm amplitude, there was no noticeable difference with a static scans. At 10 and 15 mm, the target offset was larger in the PROPELLER scan than in the 3D sequences. The amount of motion blurring also increased in the 3D sequences with larger amplitudes, but in the PROPELLER scans a discrete copy of the target appeared at approximately the inhale level.

4. Discussion

This study investigated the use of two motion-robust, radial MRI sequences, PROPELLER and 3D Vane, as primary delineation scan during online adaptive MR-guided radiotherapy of pancreatic tumors. In both the qualitative and quantitative sense, the PROPELLER images were at least on par with the conventionally used 3D T_2w scans. The PROPELLER scans presented with substantially less motion blur, but could suffer from more interslice variation compared to the 3D T_2w

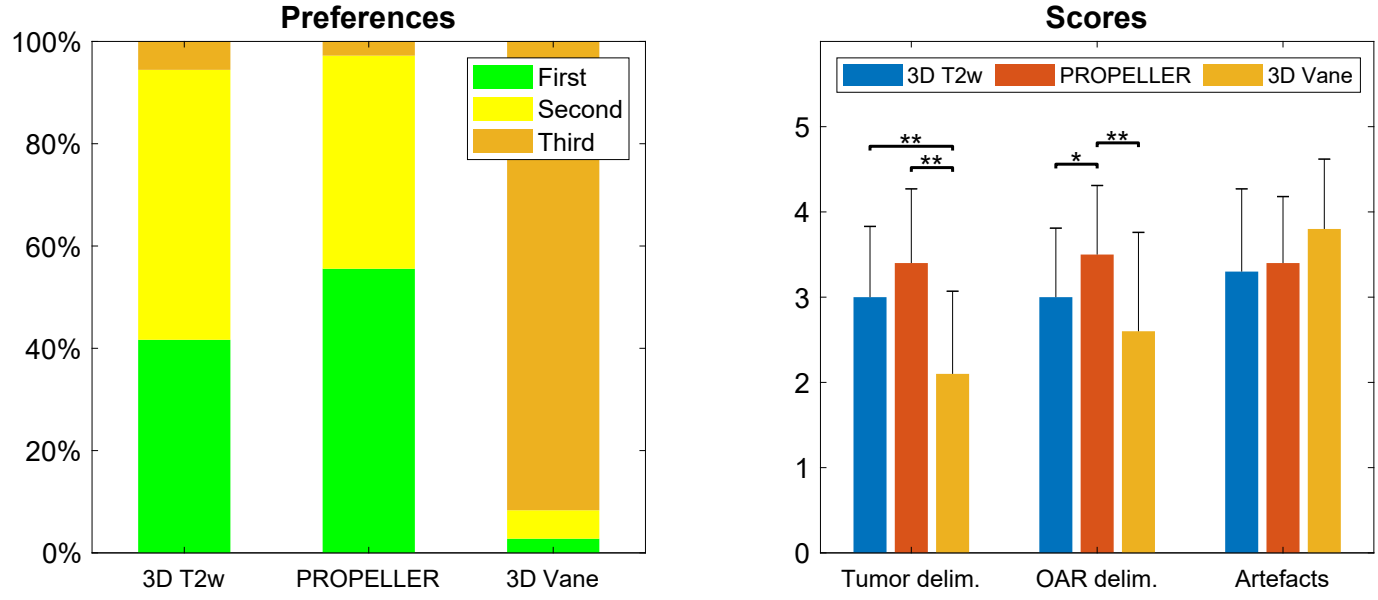

Fig. 1. The qualitative analysis results. a) The proportions of first, second and third preferences given out by the observers for each scan over all patients. b) The average scores for tumor/OAR delimitability and artifacts for each sequence. Significance markers indicate p-values below 0.05 (*) and 0.001 (**).

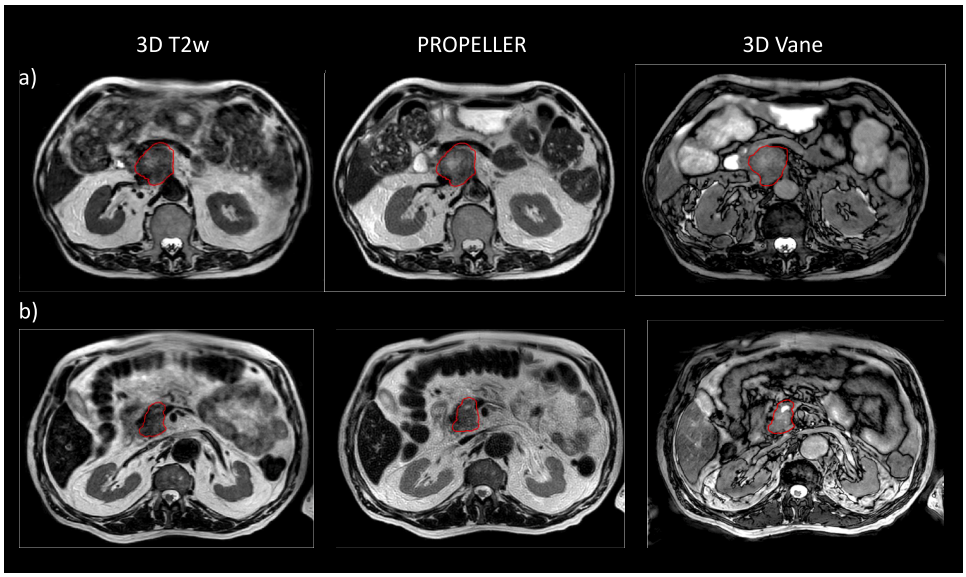

Fig. 2. Two example cases of 3D T2w, PROPELLER, and 3D Vane scans. The GTV contour is shown in red. a) A case where there was good agreement between the observers on the preference of the PROPELLER over the 3D T2w scan; b) A case where there was no clear agreement over the preference between PROPELLER and 3D T2w. The 3D Vane scan was selected as least preferred in both cases. (For interpretation of the references to colour in this figure legend, the reader is referred to the web version of this article.)

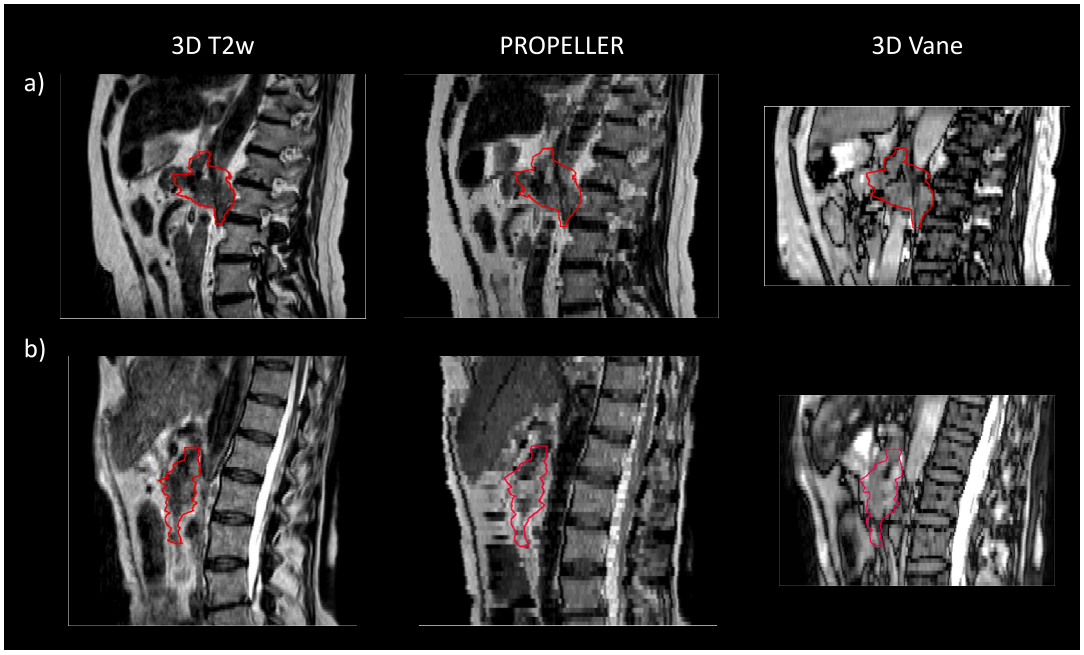

Fig. 3. Two example cases of 3D T2w, PROPELLER, and 3D Vane scans in the sagittal plane, where the interslice variability of the PROPELLER scans is demonstrated. The GTV contour is shown in red. a) A case with low interslice variability in the PROPELLER scans; b) A case with high interslice variability. (For interpretation of the references to colour in this figure legend, the reader is referred to the web version of this article.)

scans. While the 3D Vane scans were unequivocally deemed not suitable as main delineation scan, the unconventional contrast might still aid delineation as auxiliary imaging, comparable to diffusion weighted imaging.

Since the advent of MRgRT, 3D Cartesian sequences have been standard delineation scans for daily treatment delineation and adaptation on 1.5T systems, because of their high geometric fidelity, hardware compatibility, and predictable image artifacts. One should realize, however, that one of the main goals of MRgRT has always been increasing target definition accuracy, in order to safely increase target dose. In the MRgRT workflow, the uncertainty in delineation plays an increasingly important role as other geometrical errors from inter- and intrafraction motion get reduced. Due to the online adaptive setting, there is an additional time pressure for the physician to recognize and delineate the tumor and OARs. A large part of on-table time during MRgRT is taken up by contouring, especially in the upper abdomen where tumor morphology can be complex and with a large number of OARs to delineate; centers commonly report around 15 min for contouring [7,26–28]. Image quality therefore plays a crucial part in the workflow. Moreover, going by the lack of publications on this subject, we believe that the MRgRT community should explore more deeply the versatile toolbox that MRI can offer to improve visual image quality. Further investigation should also focus on the influence of image quality on interobserver delineation variability, ideally while simulating the online adaptive setting. Because this is not trivial to reliably achieve with multiple observers, assessing contouring performance was considered beyond the scope of this study.

The large interslice variability in the PROPELLER scans that was

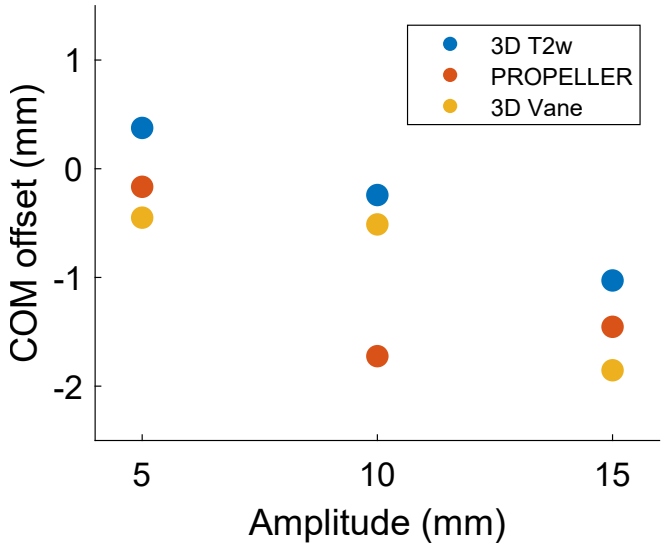

Fig. 4. The target segmentations' center of mass offset with respect to the midposition, as a function of phantom motion amplitude, for the four different scans. A positive value is towards inhale, a negative value is towards exhale.

present in some patients (Fig. 3) could be expected in a multi-2D scan, where each slice is acquired with an independent excitation and readout. This variability is probably amplified by the relatively large slice thickness compared to the 3D sequences. In this study, intrafraction motion (a probable cause of interslice variability) was already mitigated using abdominal compression to reduce tumor motion during irradiation. However, in patients where the interslice variability was especially noticeable, the observers unilaterally preferred the 3D T_2w over the PROPELLER scans. This suggests that additional measures might have to be taken to further mitigate this variability. One solution would be to acquire PROPELLER images with respiratory triggering, causing each slice to be acquired in the exhale state, but this would also introduce a positional offset in the delineations which, again, should ideally be positioned at midposition. Future real-time motion monitoring solutions during beam-on might correct for positional bias, by translating the contours based on motion measured in cine MRI. However, a triggered sequence will also prolong acquisition time. Therefore, a more viable solution might be optimizing sequence parameters like slice acquisition order and TSE shot length, in order to reduce the probability that slices are acquired in different respiratory phases.

Regarding the quantitative analysis, the gradient entropy measurements confirm that PROPELLER MRI produces images with sharper edges compared to 3D T_2w MRI. Interestingly, the 3D Vane images had the lowest gradient entropy of all four sequences. This could be due to the characteristic phase cancellation artifact at tissue boundaries where voxels contain an equal amount of water and fat [29,30]. This artifact, inherent to gradient echo sequences, results in a dark outline between different tissues, and thus a very sharp and local gradient in voxel intensity. In clinical practice, this might improve delineation accuracy in places where tissue boundaries are less visible in the primary T_2w scan. This property, and also considering the fact that 3D Vane was scored highest in terms of artifacts (Fig. 1), suggests that even though it deemed unsuitable as primary delineation scan, 3D Vane may still have a substantial clinical value in aiding the delineation process as auxiliary imaging.

The findings of the phantom COM measurements echo the results from Bertelsen et al. [25], that a target's apparent position shifts from the time-averaged position towards the median position as motion amplitude increases (Fig. 4). The results in our study suggest that this effect is more pronounced in the PROPELLER scans than in the 3D sequences. However, it should be noted that the larger slice thickness creates an uncertainty in the exact COM position, so the difference in the effect on motion in 2D and 3D sequences might not be significant. In any case, these results emphasize the importance of mitigating respiratory motion when treating pancreatic lesions, not only for dosimetric considerations but also for image quality and positional accuracy. Abdominal compression, as applied in this study, can be a simple but effective method to achieve this: we have previously reported typical intrafraction tumor respiratory amplitudes between 5 and 10 mm peak-to-peak in similar cohorts when using the same abdominal compression strategy as in this study [22,31].

There are some technical hurdles that need to be addressed when clinically implementing PROPELLER MRI in daily MRgRT. The most important consideration here is geometric fidelity. In the current clinical systems, correction for nonlinearity of the spatial encoding gradients is only performed in 2D (in-plane) for multislice 2D scans, while 3D scans are fully corrected. This means that in reality, PROPELLER slices are warped in the through-plane direction at further distances from the isocenter (>10 cm) [29]. These geometric inaccuracies could lead to systematic, nontrivial dose errors if left uncorrected [32]. This is one of the main reasons that 3D sequences were chosen as the standard scans for MR-guided radiotherapy. However, a geometric comparison between the 3D and PROPELLER sequences was purposefully omitted in this study, because a 3D correction for multislice 2D scans is currently only a software limitation. Gradient nonlinearities can be fully characterized using spherical harmonics coefficients, which enable retrospective 3D correction of both multislice 2D and 3D images. This has been performed before on the Unity MR-Linac [32], and we expect that this will become available in the standard clinical environment in the future.

To conclude, PROPELLER MRI may be a superior imaging sequence for MRgRT of pancreatic tumors. The PROPELLER sequence produces noticeably sharper in-plane images compared to the standard 3D T_2w MRIs. This improved image quality might facilitate and thereby accelerate the online treatment adaptation process, while also reducing delineation uncertainty. However, further sequence optimization before clinical implementation is warranted, to prevent large interslice variation and ensure geometric fidelity.

Declaration of Competing Interest

The authors declare that they have no known competing financial interests or personal relationships that could have appeared to influence the work reported in this paper.

Acknowledgments

This work was supported by the Dutch Cancer Foundation (KWF) under Grant Agreement no. 12665.

Appendix A. Supplementary data

Supplementary data to this article can be found online at https://doi.org/10.1016/j.phro.2023.100434.

References

[1] Raaymakers BW, Lagendijk JJW, Overweg J, Kok JGM, Raaijmakers AJE, Kerkhof EM, et al. Integrating a 1.5 T MRI scanner with a 6 MV accelerator: proof of concept. Phys Med Biol 2009;54:N229. https://doi.org/10.1088/0031-9155/54/12/N01.

[2] Raaymakers BW, Jürgenliemk-Schulz IM, Bol GH, Glitzner M, Kotte ANTJ, Van Asselen B, et al. First patients treated with a 1.5 T MRI-Linac: clinical proof of concept of a high-precision, high-field MRI guided radiotherapy treatment. Phys Med Biol 2017;62:L41. https://doi.org/10.1088/1361-6560/aa9517.

[3] Heerkens HD, Van Vulpen M, Erickson B, Reerink O, Intven MPW, van den Berg CAT, et al. MRI guided stereotactic radiotherapy for locally advanced pancreatic cancer. Br J Radiol 2018;91:20170563. https://doi.org/10.1259/bjr.20170563.

[4] Bohoudi O, Bruynzeel AME, Senan S, Cuijpers JP, Slotman BJ, Lagerwaard FJ, et al. Fast and robust online adaptive planning in stereotactic MR-guided adaptive

radiation therapy (SMART) for pancreatic cancer. Radiother Oncol 2017;125:439–44. https://doi.org/10.1016/j.radonc.2017.07.028.
[5] Rudra S, Jiang N, Rosenberg SA, Olsen JR, Roach MC, Wan L, et al. Using adaptive magnetic resonance image-guided radiation therapy for treatment of inoperable pancreatic cancer. Cancer Med 2019;8:2123–32. https://doi.org/10.1002/cam4.2100.
[6] Placidi L, Romano A, Chiloiro G, Cusumano D, Boldrini L, Cellini F, et al. On-line adaptive MR guided radiotherapy for locally advanced pancreatic cancer: clinical and dosimetric considerations. Tech Innov Patient Support Radiat Oncol 2020;15:15–21. https://doi.org/10.1016/j.tipsro.2020.06.001.
[7] Daamen LA, de Mol van Otterloo SR, van Goor IW, Eijkelenkamp H, Erickson BA, Hall WA, et al. Online adaptive MR-guided stereotactic radiotherapy for unresectable malignancies in the upper abdomen using a 1.5 T MR-linac. Acta Oncol 2022;61:111–5. https://doi.org/10.1080/0284186X.2021.2012593.
[8] Tringale KR, Tyagi N, Reyngold M, Romesser PB, Wu A, O'Reilly EM, et al. Stereotactic ablative radiation for pancreatic cancer on a 1.5 Telsa magnetic resonance-linac system. Phys Imaging Radiat Oncol 2022;24:88–94. https://doi.org/10.1016/j.phro.2022.10.003.
[9] Reyngold M, O'Reilly EM, Varghese AM, Fiasconaro M, Zinovoy M, Romesser PB, et al. Association of ablative radiation therapy with survival among patients with inoperable pancreatic cancer. JAMA Oncol 2021;7:735–8. https://doi.org/10.1001/jamaoncol.2021.0057.
[10] Ehman R, McNamara M, Brasch R, Felmlee J, Gray J, Higgins C. Influence of physiologic motion on the appearance of tissue in MR images. Radiol 1986;159:777–82. https://doi.org/10.1148/radiology.159.3.3704156.
[11] Pipe JG. Motion correction with PROPELLER MRI: application to head motion and free-breathing cardiac imaging. Magn Reson Med 1999;42:963–9. https://doi.org/10.1002/(sici)1522-2594(199911)42:5%3C963::aid-mrm17%3E3.0.co;2-l.
[12] Michaely HJ, Kramer H, Weckbach S, Dietrich O, Reiser MF, Schoenberg SO. Renal T2-weighted turbo-spin-echo imaging with BLADE at 3.0 tesla: initial experience. J Magn Reson Imaging 2008;27:148–53. https://doi.org/10.1002/jmri.21240.
[13] Nanko S, Oshima H, Watanabe T, Sasaki S, Hara M, Shibamoto Y. Usefulness of the application of the BLADE technique to reduce motion artifacts on navigation-triggered prospective acquisition correction (PACE) T2-weighted MRI (T2WI) of the liver. J Magn Reson Imaging 2009;30:321–6. https://doi.org/10.1002/jmri.21855.
[14] Hirokawa Y, Isoda H, Okada T, Arizono S, Shimada K, Yamamoto A, et al. Improved detection of hepatic metastases from pancreatic cancer using periodically rotated overlapping parallel lines with enhanced reconstruction (PROPELLER) technique after SPIO administration. Investig Radiol 2010;45:158–64. https://doi.org/10.1097/RLI.0b013e3181d32139.
[15] Rosenkrantz A, Mannelli L, Mossa D, Babb J. Breath-hold T2-weighted MRI of the liver at 3 T using the BLADE technique: impact upon image quality and lesion detection. Clin Radiol 2011;66:426–33. https://doi.org/10.1016/j.crad.2010.10.018.
[16] Nyberg E, Sandhu G, Jesberger J, Blackham K, Hsu D, Griswold M, et al. Comparison of brain MR images at 1.5 T using BLADE and rectilinear techniques for patients who move during data acquisition. Am J Neuroradiol 2012;33:77–82. https://doi.org/10.3174/ajnr.A2737.
[17] Lavdas E, Mavroidis P, Kostopoulos S, Glotsos D, Roka V, Topalzikis T, et al. Improvement of image quality using BLADE sequences in brain MR imaging. Magn Reson Imaging 2013;31:189–200. https://doi.org/10.1016/j.mri.2012.08.001.
[18] Mavroidis P, Giankou E, Tsikrika A, Kapsalaki E, Chatzigeorgiou V, Batsikas G, et al. Brain imaging: comparison of T1W FLAIR BLADE with conventional T1W SE. Magn Reson Imaging 2017;37:234–42. https://doi.org/10.1016/j.mri.2016.12.007.
[19] Sartoretti E, Wyss M, Eichenberger B, van Smoorenburg L, Binkert C, Sartoretti-Schefer S, et al. Rapid T2-weighted turbo spin echo MultiVane brain MRI using compressed SENSE: a qualitative analysis. Clin Radiol 2021;76:786–e15. https://doi.org/10.1016/j.crad.2021.06.017.
[20] Kim HG, Choi JW, Yoon SH, Lee S. Image quality assessment of silent T2 PROPELLER sequence for brain imaging in infants. Br J Radiol 2018;91:20170680. https://doi.org/10.1259/bjr.20170680.
[21] Kraus MS, Coblentz AC, Deshpande VS, Peeters JM, Itriago-Leon PM, Chavhan GB. State-of-the-art magnetic resonance imaging sequences for pediatric body imaging. Pediatr Radiol 2022. https://doi.org/10.1007/s00247-022-05528-y.
[22] Heerkens HD, Reerink O, Intven MPW, Hiensch RR, Van Den Berg CAT, Crijns SPM, et al. Pancreatic tumor motion reduction by use of a custom abdominal corset. Phys Imaging Radiat Oncol 2017;2:7–10. https://doi.org/10.1016/j.phro.2017.02.003.
[23] McGee KP, Manduca A, Felmlee JP, Riederer SJ, Ehman RL. Image metric-based correction (autocorrection) of motion effects: analysis of image metrics. J Magn Reson Imaging 2000;11:174–81. https://doi.org/10.1002/(SICI)1522-2586(200002)11:2%3C174::AID-JMRI15%3E3.0.CO;2-3.
[24] Wolthaus JW, Sonke JJ, van Herk M, Belderbos JS, Rossi MM, Lebesque JV, et al. Comparison of different strategies to use four-dimensional computed tomography in treatment planning for lung cancer patients. Int J Radiat Oncol Biol Phys 2008;70:1229–38. https://doi.org/10.1016/j.ijrobp.2007.11.042.
[25] Bertelsen A, Bernchou U, Schytte T, Brink C, Mahmood F. The effect of respiration-induced target motion in 3D magnetic resonance images. Phys Imaging Radiat Oncol 2022;24:167–72. https://doi.org/10.1016/j.phro.2022.11.010.
[26] Paulson ES, Ahunbay E, Chen X, Mickevicius NJ, Chen GP, Schultz C, et al. 4D-MRI driven MR-guided online adaptive radiotherapy for abdominal stereotactic body radiation therapy on a high field MR-Linac: implementation and initial clinical experience. Clin Transl Radiat Oncol 2020;23:72–9. https://doi.org/10.1016/j.ctro.2020.05.002.
[27] Stanescu T, Shessel A, Carpino-Rocca C, Taylor E, Semeniuk O, Li W, et al. MRI-guided online adaptive stereotactic body radiation therapy of liver and pancreas tumors on an MR-Linac system. Cancers 2022;14:716. https://doi.org/10.3390/cancers14030716.
[28] de Leon J, Crawford D, Moutrie Z, Alvares S, Hogan L, Pagulayan C, et al. Early experience with MR-guided adaptive radiotherapy using a 1.5 T MR-Linac: first 6 months of operation using adapt to shape workflow. J Med Imaging Radiat Oncol 2022;66:138–45. https://doi.org/10.1111/1754-9485.13336.
[29] Bernstein MA, King KF, Zou XJ. Handbook of MRI pulse sequences. Burlington: Elsevier; 2004.
[30] Brown RW, Cheng YCN, Haacke EM, Thompson MR, Venkatesan R. Magnetic Resonance Imaging: Physical Principles and Sequence Design. 2nd ed. Hoboken: John Wiley & Sons, Inc.; 2014.
[31] Grimbergen G, Eijkelenkamp H, Heerkens HD, Raaymakers BW, Intven MP, Meijer GJ. Intrafraction pancreatic tumor motion patterns during ungated magnetic resonance guided radiotherapy with an abdominal corset. Phys Imaging Radiat Oncol 2022;21:1–5. https://doi.org/10.1016/j.phro.2021.12.001.
[32] Keesman R, van de Lindt TN, Juan-Cruz C, van den Wollenberg W, van der Bijl E, Nowee ME, et al. Correcting geometric image distortions in slice-based 4D-MRI on the MR-linac. Med Phys 2019;46:3044–54. https://doi.org/10.1002/mp.13602.